Journal of Vacuum Science and Technology A

RESEARCH ARTICLE | SEPTEMBER 05 2025

Microwave enhanced atomic layer deposition (MW-ALD): Incorporating a microwave antenna into an ALD system and performing *in situ* direct microwave exposure during ALD

Special Collection: Atomic Layer Deposition (ALD)

Benjamin Kupp; Jessica Haglund ; Shane Witsell ; Mohammad Kamarehi; John F. Conley, Jr.

J. Vac. Sci. Technol. A 43, 052403 (2025)
https://doi.org/10.1116/6.0004633
CHORUS

JVST A
Journal of Vacuum Science & Technology A

ARTICLE

pubs.aip.org/avs/jva

Microwave enhanced atomic layer deposition (MW-ALD): Incorporating a microwave antenna into an ALD system and performing *in situ* direct microwave exposure during ALD

Cite as: J. Vac. Sci. Technol. A **43**, 052403 (2025); doi: 10.1116/6.0004633
Submitted: 7 April 2025 · Accepted: 8 August 2025 ·
Published Online: 5 September 2025

Benjamin Kupp,[1] Jessica Haglund,[2] Shane Witsell,[2] Mohammad Kamarehi,[3] and John F. Conley, Jr.[1,2,a)]

AFFILIATIONS

[1]Department of Materials Science, Oregon State University, Corvallis, Oregon 97331
[2]School of Electrical Engineering and Computer Science, Oregon State University, Corvallis, Oregon 97331
[3]MKS Instruments, Plasma & Reactive Gas Solutions, 90 Industrial Way, Wilmington, Massachusetts 01887

Note: This paper is part of the Special Topic on Atomic Layer Deposition (ALD).
[a)]**Author to whom correspondence should be addressed:** jconley@eecs.oregonstate.edu

ABSTRACT

Self-limiting, purge-separated, cyclic reactions enable atomic layer deposition (ALD) to produce highly uniform and conformal films with precise thickness control. However, the typical relatively low deposition temperatures can lead to residual impurities, defects, and suboptimal material properties. To address this, we introduce microwave enhanced ALD (MW-ALD), an energy enhanced ALD technique in which *in situ* microwave exposure is included in each ALD cycle. The design of the microwave antenna and exposure system and integration into a commercial ALD chamber are first described. The benefits of MW-ALD are then demonstrated using Al_2O_3, a material that in bulk form is not expected to strongly interact with microwaves. Through ellipsometry and electrical measurements, we show that *in situ* MW irradiation annealing can reduce thickness, improve film properties such as refractive index, reduce high field current leakage, and improve breakdown strength. In all cases, MW-ALD produced a greater change in properties than was produced by an equivalent microwave exposure performed post deposition.

I. INTRODUCTION

Atomic layer deposition (ALD) is based on alternating purge-separated self-limiting surface reactions so that films are deposited in a layer-by-layer fashion. Inherent advantages of ALD include the atomic scale controlled growth of highly uniform and conformal thin films at relatively low temperatures (<300 °C). A low thermal budget is often critical in semiconductor fabrication for back-end-of-line processing, 3D integration, avoiding unwanted diffusion, and maintaining stable device parameters in metal/insulator/metal (MIM) and metal/oxide/semiconductor (MOS) devices. Low thermal budget is also necessary for deposition on glass or flexible substrates for large area electronics. While advantageous for these applications, the low deposition temperatures typical of ALD can lead to incorporation of excess –OH groups or other residual impurities from unreacted ligands.[1] These impurities can result in poor stoichiometry and suboptimal physical, optical, and electrical properties.[2] Increasing the deposition temperature can reduce impurities, improve stoichiometry, and improve properties, but may move a process out of the ALD window and into the chemical vapor deposition (CVD) regime, negating many of the benefits of ALD.[3] Therefore, postdeposition annealing (PDA) at elevated temperatures is often necessary to improve ALD films.[4] However, the PDA temperatures that are typically required can exceed the maximum temperature limitations of the substrate or previously formed electronics.

To maintain the advantages of self-limiting ALD while maximizing film properties, *in situ* treatments, such as annealing or adding other forms of energy during each (or every few) ALD deposition cycle(s) or supercycle(s), can help drive/speed reactions and reduce impurity/ligand incorporation. The first demonstration of

this approach incorporated *in situ* rapid thermal anneals into a standard ALD cycle and was called modulated temperature ALD.[5–8] Improvements in film density, refractive index, leakage, and relative dielectric constant were demonstrated that could not be achieved by postdeposition annealing alone, even at a higher temperature. Since then, in addition to *in situ* annealing (also known as dep/anneal/dep/anneal or DADA),[9–14] much work has explored other approaches such as flashlamp annealing[15,16] and periodic exposure plasma (a.k.a. atomic layer annealing or DSDS),[17–26] UV (a.k.a. DUDU) exposure,[12,27–32] lasers,[33] and electric fields.[34] We will collectively refer to techniques in which the addition of energy during ALD *enhances*, *rather than enables* (such as electron beam enabled ALD,[35] etc.), an ALD process as energy enhanced ALD (EE-ALD). Note that these EE-ALD methods are distinct from plasma enhanced ALD (PEALD), an excellent review of which can be found in Ref. 36.

Documented benefits from the various methods of EE-ALD include increased density, increased dielectric constant, increased refractive index, higher GPC, reduced leakage, reduced residual impurities, reduced defects, and improved crystallinity, all at a lower thermal budget than and often not achievable by PDA, even PDA at higher temperatures.[6,8,10–15,17–19,23,28,31,37] The reason that EE-ALD films show improved properties is that the *in situ* treatments (RTA, UV, plasma, etc.) are able to remove impurities and defects from the surface of the growing film *before* they can become buried, resulting in a more complete densification or purification.[6,17,22,23] PDA, on the other hand, can only partially densify a film by driving off residual impurities within a diffusion length or so of the surface. Impurities beyond a diffusion length from the surface can become effectively trapped so that they cannot be completely removed by postdeposition treatments. One downside of current EE-ALD techniques is the additional time these extra steps add to the ALD cycle, particularly the cooldown time when *in situ* thermal annealing is used.[6,8] Other potential downsides, depending on the EE-ALD method, include plasma damage and UV damage, which can both result in defects and charge trapping.[20,38]

An alternative way of supplying energy for EE-ALD is microwaves. Microwaves heat materials through ohmic (resistive) conduction and dielectric polarization loss, but can also interact through nonthermal mechanisms.[39] Resistive heating is the primary mechanism in conductive materials and can also be used to heat adjacent nonconductive films. Polarization heating occurs in dielectrics. The loss tangent, $\tan\delta = \varepsilon''/\varepsilon'$, where ε' and ε'' are the real and imaginary components of the dielectric constant, describes how well MWs couple with a given material, where δ represents the phase lag between the applied electric field of the MW and the electric dipoles present in dielectric materials. This phase lag occurs when dipoles are unable to reorient sufficiently quickly in response to the frequency of the applied electric field. A large loss tangent indicates strong coupling and energy absorption by the material.[40] The nonthermal mechanisms are still a subject of research and debate,[39] but studies have shown improved results using microwave annealing at nominally the same (or lower temperatures) as (than) thermal heating, possibly due to the direct interaction of microwaves with defects, including point defects. For example, microwaves have demonstrated advantages over conventional thermal PDA such as reduced temperatures for dopant activation without diffusion, recrystallization, healing plasma damage, and even for growing nanowires.[41–46] Postdeposition and postmetallization microwave annealing (without plasma generation) have also been shown to improve thin film material quality and device performance at lower thermal budget.[39,45–53] The mechanism of microwave interaction in these studies has been attributed not only to thermal effects but also nonthermal effects (not involving bulk heating) such as direct interaction of microwave radiation with defect dipoles in the film.[54] *Postdeposition* microwave annealing has even been applied to fully formed ALD films and devices.[51,55,56] However, there are no reports of using a microwave source in the deposition chamber for *in situ* annealing *during* deposition.

To address the limitations and shortcomings of the existing EE-ALD methods, we introduce microwave enhanced ALD (MW-ALD) in which MW exposures are performed during each deposition cycle. A key potential benefit of MW-ALD is the selective targeting of polarizable defects and impurities, which should allow their removal from the growing film without excessive substrate heating, maintaining a low thermal budget and minimizing impact to cycle times. In this work, we describe the design of a MW exposure system and its implementation into a commercial ALD chamber. We then demonstrate the effect of MW-ALD on Al_2O_3, a material with a low loss tangent that in bulk form is not expected to interact strongly with microwaves. Preliminary results are presented on the impact of *in situ* MW exposures on thickness, refractive index, and electrical properties and are compared with equivalent MW exposures performed post deposition.

II. MICROWAVE DESIGN AND INTEGRATION

The MW system and custom antenna was designed and developed with MKS instruments, and initial functional testing was performed at MKS. The design considerations included geometric constraints, power requirements, and environmental conditions. Prior to the construction of a prototype, proprietary COMSOL simulations were performed to guide the design. Based on the internal geometry of the Picosun SUNALE R-200 ALD chamber, a frequency range of 2.4–2.5 GHz was identified for maximum MW power coupling with a target substrate. The wavelength, λ, of 12.23 cm was several times less than the internal diameter of the chamber and allowed for energy propagation, despite any standing waves created by reflection from the chamber walls. A critical factor in this process was ensuring uniform MW exposure across the substrate size range using a physically compatible antenna. A helical antenna design was selected (over alternatives such as horn and dipole antennae) based on three major considerations: (1) helical antennae have a narrow and elongated cylindrical form factor at the 2.45 GHz operating frequency, making them well suited for fitting in the vacuum access port of the R200 chamber, (2) they enable greater directional radiation precision over the other designs with radiation directivity and gain determined by the number of turns, and (3) they have only a real or resistive component of input impedance with no reactive element to tune out, permitting system tuning directly through adjustment of the operating frequency. This last consideration is highly important when coaxial cables are employed within the power delivery system to avoid standing waves and, therefore, excessive and nonuniform heating.[57–60]

The primary design elements of the helical antenna consisted of a frequency of 2.450 GHz, copper material for the ease of mechanical formation and high electrical conductivity, five turns with a diameter of 1.540 in. per turn and a total height of 6.025 in., an effective gain of 15.17, and a half-power band width of 46.32° providing sufficient angular exposure. The distance, d, between the end of the helical antenna and the surface of the deposition substrate was approximately 43 cm. This distance assured far-field radiation over the processing sample [where the wave propagation becomes an identifiable TEM (transverse electro-magnetic) mode] and enabled more uniform exposure of the sample. For far-field, d should be greater than $2D^2/\lambda$, where D is the largest dimension of the antenna and λ is the wavelength of the microwave radiation.

Due to a typical chamber processing pressure of around 6 Torr and microwave frequency of around 2.45 GHz, unwanted plasma formation around the antenna was a concern.[61] To suppress plasma formation, the MW antenna was housed in a quartz jar that was sealed against the vacuum chamber and backed to atmosphere through a small vent. The final antenna prototype is shown in Fig. 1(a). A simulation of the typical radiation pattern from a helical antenna is shown in Fig. 1(b).

The R200 was originally designed with a remote plasma source and included plasma guiding cones in the interior chamber [Fig. 1(c)]. To accommodate the MW antenna, the plasma source and plasma guiding cones were removed. Figure 1(d) shows the placement of MW antenna in the vacated plasma port. The removal of the cones opened the small, previously contained deposition space to the entire vacuum chamber. Even with extended purging times, there were signs of nonideal ALD film growth that proved difficult to completely remove.

A block diagram of the MW system is shown in Fig. 2. The path from the 1 kW solid state microwave generator (MKS SG1024) to the antenna includes an integrated coax to waveguide isolator designed by MKS, a typical three-stub tuner, a waveguide to coaxial transition, and a dual coaxial directional coupler (Werlatone). The microwave generator was connected to the R200's console, enabling precise and synchronized software controlled MW exposure windows. Power sensors were connected to both the dual directional coupler and the integrated isolator for monitoring forward and reflected power, respectively. The integrated isolator protects the microwave generator by absorbing reflected power from the antenna in case there is a large impedance mismatch. The stub tuner is a redundant tuning method that was included in case frequency tuning alone was insufficient. The dual directional coupler provides a connection point for both power sensors, though the integrated isolator was more accurate for monitoring the reflected power since the reverse traveling wave was terminated in a matched load and, therefore, the measurements were not influenced by the directivity of the coupler. Where components were not directly connected to one another, coaxial cables (CAVO 5228) with 7/16 in. connectors were used.

The final step in integrating the MW source was tuning the MW system after installation in the R200 chamber. Though COMSOL modeling had provided an ideal estimated frequency range, the actual optimum operating frequency had to be determined

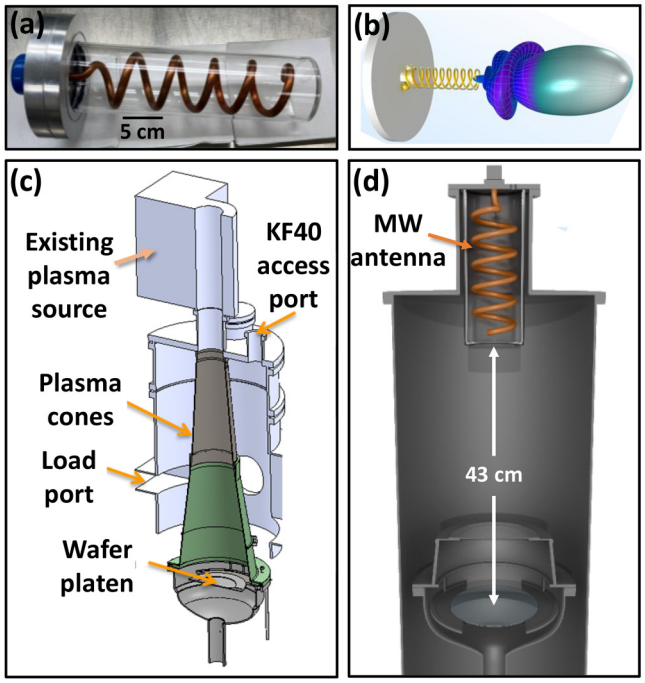

FIG. 1. (a) Photograph of the actual microwave antenna enclosed in a quartz jar backed to the atmosphere and (b) typical simulated radiation pattern. Cartoon schematic illustrations of the Picosun R200 Advanced ALD chamber (c) with original plasma cones and (d) modified with an MW antenna. The distance from the antenna to the sample surface is indicated.

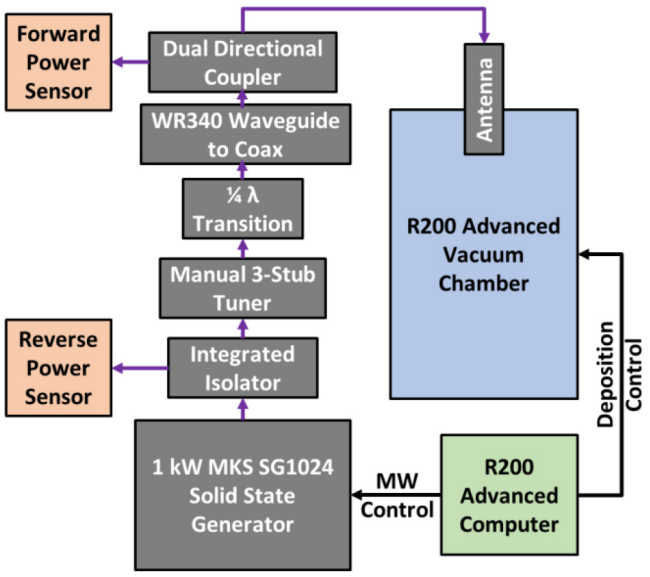

FIG. 2. MW system block diagram identifying the components comprising the pathway from the MW generator to the antenna. Color of box indicates computer control (green, bottom right box), R200 ALD chamber (blue, large box, top right), power sensors (orange, left column), and MW generation and transmission to antenna (gray, central column).

empirically by measuring the forward and reflected power across a range of frequencies and selecting the point at which the reflected to forward power ratio was minimized. During the tuning process, the generator output, P_{out}, was fixed at 50 W. However, due to the 50 dB scaling factor present in a dual directional coupler, the actual measured forward power was only around 500 μW. Tuning was carried out by adjusting frequency output of the SG1024 solid-state generator from 2.4 to 2.5 GHz. As expected, the manual 3-stub tuner was not required for tuning, validating the choice to use a helical antenna. The measured forward power, reflected power, and forward/reflected power ratio versus microwave frequency are shown in Fig. 3. The global maximum at 2.414 GHz identified the optimal frequency. This frequency was then used for all MW exposures to limit energy loss in the MW delivery circuit and reduce overheating of the transmission components.

During the integration process, safety was a primary concern as the R200 chamber was not designed for MW containment. While vacuum tight, the chamber was not perfectly MW tight. To prepare for MW annealing, the stainless-steel vacuum chamber was sealed and grounded, viewports were replaced with blank stainless-steel flanges, junctions were wrapped in an RF shielding tape, and aluminum foil was used for persistent MW leaks. Thus modified, it was able to prevent most radiation leakage. According to the National Institute of Standards and Technology, the maximum MW occupational exposure limit is around 8 mW/cm^2 for a 2.4 GHz signal.[62] A handheld RF meter (Extech Instruments) indicated that MW leakage was below this limit at $P_{out} = 400$ W. At $P_{out} = 400$ W, the calculated power density at the sample surface, $P_{sample} = P_{out} * G / 4\pi * d^2$, where G is the linear gain of 15.17 and the distance, d, is 43 cm, was approximately 250 mW/cm^2.

III. EXPERIMENTAL DETAILS

Al_2O_3 was deposited using both standard thermal ALD and MW-ALD. Both were performed on a modified 200 mm plasma enhanced PE-ALD hot wall system (Picosun SUNALE R-200). Trimethylaluminum (TMA) (Sigma Aldrich, 97%) was used as the metal precursor with de-ionized H_2O as the coreactant. Depositions were carried out at chamber setpoints of 100 and 300 °C, resulting in actual wafer temperatures of 88 and 238 °C measured using a SensArray Corporation Thermocouple Instrumented Wafer P/N 1530A-6-0201 (see the supplementary material). The process gas was N_2, flowing at a total rate of 900 SCCM. The base chamber pressure during deposition was between approximately 5 and 6 Torr. The minimum system pulse time of 0.1 s was used for both TMA and H_2O. Due to chamber configuration modifications necessitated by the installation of the MW antenna (discussion above), long purge times were required. For the 238 °C depositions, a N_2 purge time of 60 s was used for both TMA and H_2O. Deposition at 88 °C required extending both purge times to 120 s.

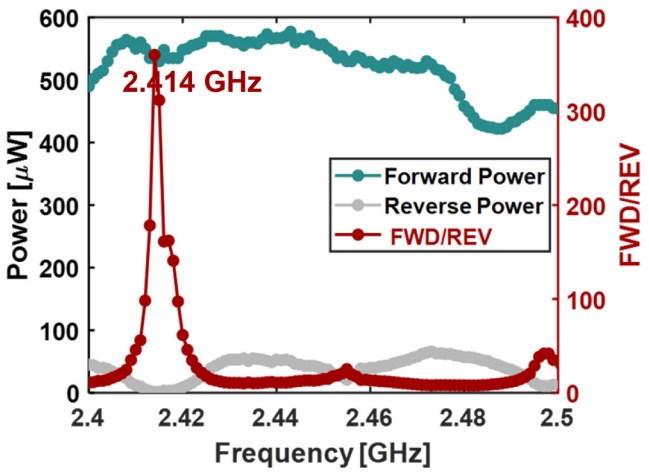

FIG. 3. Plot of forward (blue, top data) and reflected (gray, bottom data) MW power vs frequency power on the left axis and the reflected/forward power ratio (red, peaked data) on the right axis.

MW exposure was performed *in situ* using a custom helical antenna driven by a 1 kW solid state microwave generator (MKS SG1024) through a matching network consisting of an integrated coax to a waveguide isolator designed by MKS, a typical three-stub tuner, a waveguide to coaxial transition, and a dual directional coupler (Werlatone). MW exposure was performed *in situ*, either during or immediately after (post) ALD deposition. When performed during ALD, 400 W MW exposures of 30 s duration were incorporated into either the TMA or H_2O purging step of every ALD cycle, beginning approximately 5 s after the end of the precursor pulse. This is referred to as MW-ALD. The 5 s delay was included to allow purging so as to avoid direct interaction with gaseous species. The data presented focus on MW exposure incorporated during the TMA purges as this showed a larger impact on film properties than MW exposure during the water purge.

On other samples, postdeposition MW exposures were performed at the end of the deposition, without breaking vacuum, and referred to as MW-PDA. To replicate the same total MW exposure and timing and avoid differences in heating, MW-PDA exposures comprised a train of 30 s MW pulses with one pulse for each cycle spaced every 120 s or 240 s for depositions at 238 and 88 °C, respectively. ALD deposition sequences are illustrated in Fig. 4.

Al_2O_3 films were deposited on n-type (88) Si substrates with 2.4 nm of native SiO_2. Film thickness and refractive index (RI) were mapped across 125 mm wafers using a multiwavelength mapping ellipsometer with an XY stage (Filmsense FS-1).

Metal-oxide-semiconductor (MOS) devices were fabricated by thermally evaporating aluminum through a shadow mask to create top gate electrical contacts (Veeco 7700). The bottom contact (Si substrate) was fabricated using an indium solder on the corner of each coupon. Current–voltage measurements were taken using a semiconductor parameter analyzer (Agilent B1500 A) and conducted using a probe station (Cascade Alessi REL-4800) in a dark box.

IV. EXPERIMENTAL RESULTS

A. Impact of MW exposure on physical properties

Figure 5 shows maps of ellipsometric film thickness for 100 cycle Al_2O_3 films deposited on 25 × 25 mm^2 coupons at 88 or 238 °C using three different MW exposure conditions: (1) standard thermal ALD control (no MW exposure), (2) MW-ALD (*in situ* MW exposure during every ALD cycle), and (3) MW-PDA

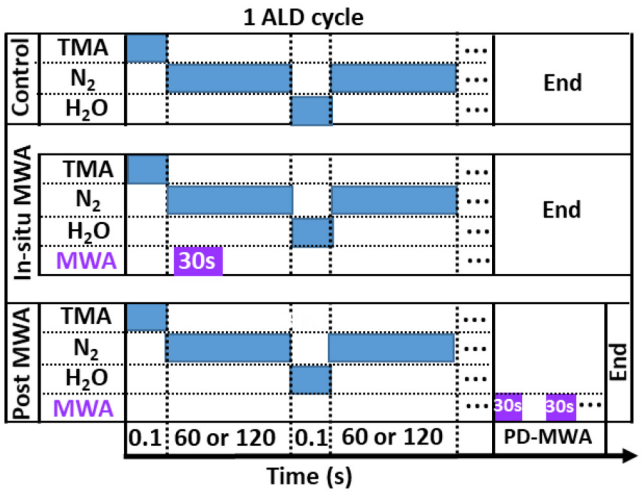

FIG. 4. Illustration of ALD pulse sequences and MW exposures for control, MW-ALD, and MW-PDA conditions.

(thermal ALD + postdeposition MW exposure). A cumulative distribution plot of all the thickness points from these maps is shown in Fig. 6(a). Figure 6(b) shows a similar plot of thickness points for 200 cycle films deposited at 238 °C. In addition to displaying all data points, cumulative distribution plots allow visual identification of uniformity (indicated by slope) and distinction of small differences in average thickness for even overlapping distributions. For the 100 cycle standard thermal ALD control film deposited at 238 °C [Fig. 6(a)], the median thickness was 9.6 nm. (Thickness maps and thickness variation of control wafers are shown in Figs. S1 and S2 in the supplementary material.) The median thickness of the MW-ALD film, incorporating *in situ* MW exposure during every TMA purge step, was 8.6 nm, a reduction in thickness of ~10% versus standard thermal ALD. For the MW-PDA film, in

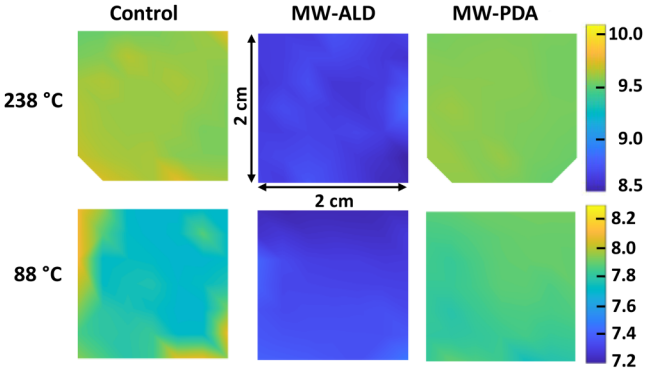

FIG. 5. Ellipsometric film thickness maps for 100 cycle films deposited at either 88 or 238 °C via either standard thermal ALD (control), MW-ALD, or standard thermal ALD + MW-PDA.

which the same aggregate MW exposure was performed immediately after the end of the deposition without breaking vacuum, there was little change in median thickness. When the MW exposure was included during the H_2O purge rather than the TMA purge, a much reduced impact on film thickness was observed (~2.5% vs ~10% reduction, respectively).

Similar results were seen for 200 cycle depositions at 238 °C [Fig. 6(b)]. The median thickness of the 200 cycle control film was 20.0 nm with a refractive index of 1.72, approximately what was expected for these process conditions.[2] For the MW-ALD process, there was again a ~10% reduction in median thickness to 18.0 nm and a slight increase in refractive index to 1.74. Both the reduction in thickness and increase in RI are consistent with film densification. The median thickness of the MW-PDA film was slightly

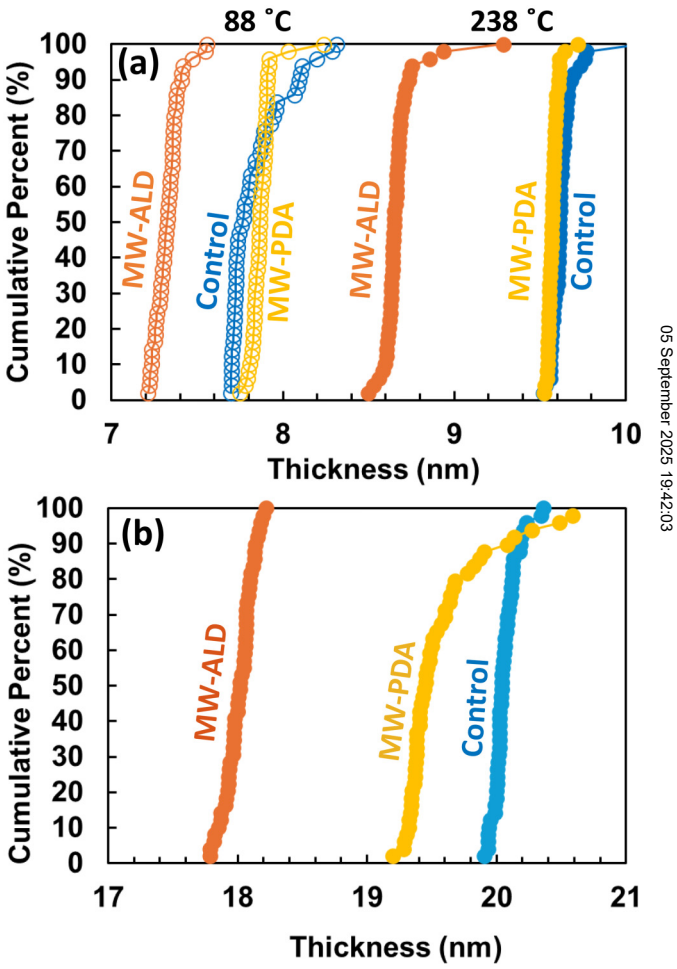

FIG. 6. Cumulative percentage plots of Al_2O_3 film thickness for (a) 100 cycle films deposited at 88 °C (open circles) and 238 °C (filled circles) and (b) 200 cycle films deposited at 238 °C. Each data set comprises 49 sites mapped across a 25 mm × 25 cm wafer. Shown for each deposition condition are control (no MW exposure, blue), MW-PDA (postdeposition MW exposure, yellow), and MW-ALD (*in situ* every cycle MW exposure, orange).

TABLE I. Summary of ellipsometry data.

Deposition temperature (°C)	Cycles	Control Median thickness/std (nm)	Control RI	MW-ALD Median thickness (nm)	MW-ALD RI	MW-PDA Median thickness (nm)	MW-PDA RI
88	100	7.8/0.2	—	7.3	—	7.9	—
238	100	9.6	—	8.6	—	9.6	—
	200	20.0	1.72	18.0	1.74	19.5	1.72

lower than the control at 19.5 nm, a 2.5% reduction, but the refractive index was essentially unchanged at 1.72.

A qualitatively similar impact of MW exposure was seen for depositions at 88 °C [Fig. 6(a)]. At 88 °C, the median thickness of the 100 cycle control film was 7.8 nm while the MW-ALD film was 7.3 nm, a thickness reduction of ~6.5%. The MW-PDA had a median thickness of 7.9 nm, little change versus the control. Ellipsometry results are summarized in Table I.

B. Impact of MW exposure on current leakage and dielectric breakdown

Shown in Fig. 7 are (a) current density (J) vs electric field (E) curves and (b) extracted breakdown fields for Al/Al_2O_3/Si MOS devices with 100 cycle Al_2O_3 layers deposited at 88 °C using the control, MW-ALD, and MW-PDA sequences. Ten devices of each type were tested. Relative to the control, the MW-ALD treatment resulted in a slight increase in low field leakage but reduced the high field leakage by more than an order of magnitude and increased the median breakdown field strength by almost 0.5 MV/cm. The MW-PDA device, despite showing little change in film thickness and refractive index, also showed improvement over the control, with leakage and breakdown generally between the control and MW-ALD films. This exemplifies the sensitivity of electronic properties to even small changes in material morphology/composition.

V. DISCUSSION

To estimate the thermal cycling during MW exposure, a thermocouple (TC) instrumented wafer and temperature stickers were used to monitor wafer temperature during MW exposure sequences equivalent to those used above. These measurements are described fully in the supplementary material. Although the TC wafer produced unreliable results during and for some time after MW exposure, relevant data was obtained (see Fig. S1 in the supplementary material). It was found that the wafer heats up a little during the MW exposure and then cools down partially to fully between exposures. Note that the conductivity of the TC wafer could not be determined, and as resistive MW heating depends on conductivity, the coupons used for actual depositions may behave slightly differently.

For the 88 °C baseline depositions, the maximum wafer temperature, reached immediately at end of MW exposure, was between ~6 to less than 10 °C above baseline (~93–~97 °C), likely closer to ~7 °C. The wafer was able to cool back to baseline after each MW exposure and experienced a less than 1 °C overall increase in wafer temperature after 20 cycles (see Fig. S2 in the supplementary material). The 88 °C baseline MW-ALD deposition was thus likely conducted at an average temperature of ~3–5 °C higher than the thermal ALD control.

For the 238 °C baseline depositions, the maximum wafer temperature was between ~17 to less than 23 °C above baseline (255 to

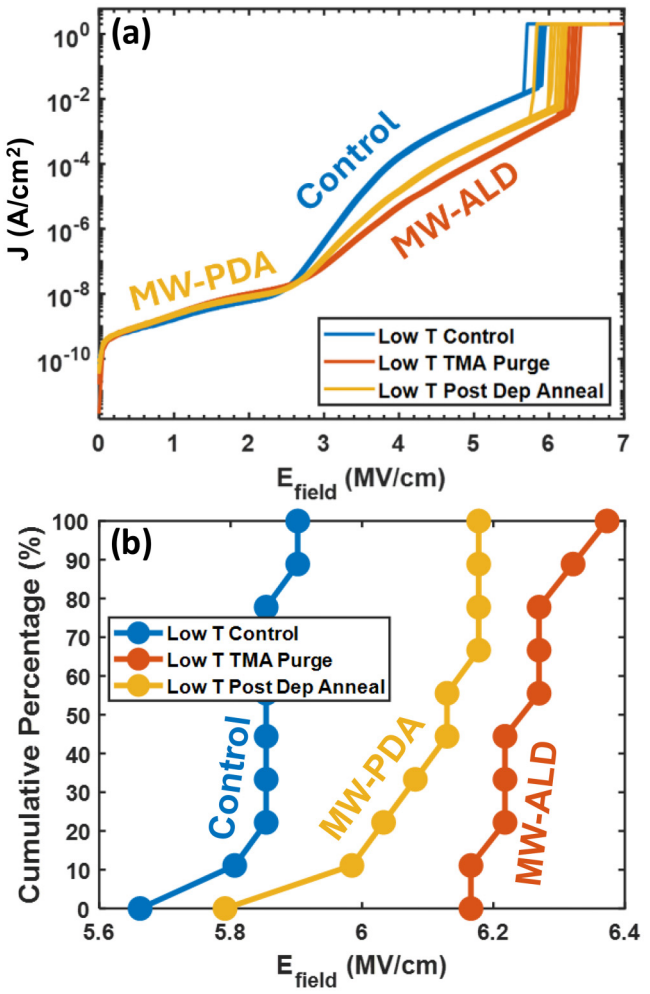

FIG. 7. (a) Log(J) vs E_{field} curves and (b) cumulative plot of extracted breakdown fields of Al/Al_2O_3/Si MOS devices for 100 cycle Al_2O_3 layers deposited at 88 °C using either the control, MW-ALD, or MW-PDA process sequence. Each MW treatment condition is represented by ten devices. J–E curves are normalized by thickness and contact area.

less than 260 °C), but likely much closer to ~17 °C (see Fig. S3 in the supplementary material). As the cooling time was shorter, the wafer temperature did not cool all the way to baseline between MW exposures, resulting in an ~8.5 °C overall increase in wafer temperature after 100 cycles, saturating between 20 and 50 cycles (see Fig. S3 in the supplementary material). The 238 °C baseline MW-ALD deposition was thus likely conducted at an average temperature of 10–12 °C higher than the thermal ALD control.

The overall heating of the TC wafer during the MW-ALD process was thus fairly small, particularly for the 88 °C baseline depositions. Heating is dominated by resistive heating of the Si substrate and is independent of the position of the MW exposure in the ALD cycle. However, the peak and average wafer temperature will be slightly higher during the purge that contains the MW exposure. The average temperature during the TMA purge was likely higher than the H_2O purge by about 3 °C and 4–5 °C for the 88 and 238 °C baseline depositions, respectively. Despite these very small temperature differences, when the equivalent MW exposure was included during the H_2O purge rather than the TMA purge, a much reduced impact on film thickness was observed (~2.5% vs ~10% reduction, respectively). The clear influence of MW exposure on film properties, despite these small temperature differences, makes it unlikely that the mechanism of MW interaction is purely thermal. Instead, the differences appear at least partially attributable to nonthermal effects such as direct MW coupling with a (likely) polarizable species only present during the TMA purge part of the cycle.[39,44,45,63]

In all cases, MW-ALD produced a greater change in film properties than that produced by an equivalent microwave exposure performed post deposition (MW-PDA). This also points to a surface related interaction mechanism. This result is consistent with what has typically been reported for other EE-ALD techniques—that incorporation of *in situ* energy into the ALD cycle produced benefits that could not be matched by postdeposition treatment alone.[6,8,10–15,17–19,23,28,31,37] As reported for other EE-ALD techniques, it is likely that adding the microwave energy during rather than after the ALD process may allow for more efficient removal of defects and impurities/unreacted ligands from the surface of the growing film before they can become buried by subsequent layers. Future work will compare carbon content in MW-ALD, MW-PDA, and standard thermal ALD films.

Due to a less-ideal ALD deposition at the lower temperature with potentially more defects and impurities available for MW coupling,[2] it was hypothesized that MW-ALD at 88 °C might yield greater changes in film properties than for the corresponding deposition at 238 °C. However, this did not appear to be the case for the ALD Al_2O_3 process here. One possible explanation is the slightly greater MW heating at 238 °C due to less cooling for the 60 s vs 120 s purges at 238 °C vs 88 °C, respectively. More work will be necessary to better characterize the relative contributions of thermal versus nonthermal microwave effects, such as direct comparisons of depositions performed at 88 vs 94 °C and 238 vs 255 °C.

VI. SUMMARY AND CONCLUSIONS

In this work, we described the design and development of a MW antenna and exposure system and its integration into a standard commercial ALD chamber. This system was shown to be capable of providing precisely controlled, *in situ* MW exposure during every ALD cycle, *without* generation of plasma. Microwave enhanced ALD (MW-ALD) with *in situ* MW irradiation exposure in each ALD cycle was performed using TMA and H_2O. Using ellipsometry and electrical measurements, it was demonstrated that MW-ALD can reduce thickness and improve film qualities not only over standard thermal ALD but also over an equivalent microwave exposure performed post deposition. As compared to standard thermal ALD, adding an *in situ* ~250 mW/cm^2 MW exposure (without plasma generation) during the TMA purge part of each ALD cycle resulted in a reduction in median Al_2O_3 film thickness by ~6.5% and ~10% across a 25 mm × 25 mm Si coupon for depositions at 88 and 238 °C, respectively, accompanied by a slight increase in the optical refractive index. Preliminary current versus voltage measurements on Al/Al_2O_3/Si devices showed a reduction in high field leakage and an increase in breakdown strength with a slight increase in low field leakage. In all cases, MW-ALD produced greater changes than an equivalent MW exposure performed after deposition (MW-PDA).

Thermocouple and temperature sticker measurements showed that the MW exposure used for the 88 and 238 °C depositions resulted in a <1 °C and ~8.5 °C overall heating of the wafer and that MW-ALD depositions were likely conducted at an average temperature of 3–5 °C, 8–12 °C higher than the thermal ALD control, respectively. The average temperature during the TMA purge (containing the MW exposure), was likely higher than the H_2O purge by about 3 °C and 4–5 °C for the 88 and 238 °C baseline depositions, respectively. Despite the small wafer temperature differences, a much reduced impact on Al_2O_3 film thickness occurred when the same MW exposure was included during the H_2O purge, rather than the TMA purge step, even for a low loss tangent material like Al_2O_3 that is not expected to strongly interact with microwaves.[64] This points to a role for direct non-thermal MW interaction with species on the surface of the growing film.[39,44,45,63]

Although *post*-deposition MW annealing had previously been demonstrated to positively impact material and device properties,[39,45–53] this is the first demonstration that MW exposures performed *during* every ALD cycle can further improve Al_2O_3 film properties. While the purge times used here may be untenable for high throughput manufacturing, purpose-built chambers designed to more efficiently deliver higher MW power could provide sufficient MW exposure with the addition of minimal extra processing time. It is also likely that due to the low growth per cycle of ALD, microwave exposure in every cycle may not be necessary. Finally, other materials (polarizable oxides such as ZnO) and precursor chemistries may be more amenable to MW interaction than Al_2O_3.

The *in situ* addition of energy to relatively low temperature ALD processes via EE-ALD techniques may be necessary to approach *ideal* ALD more closely and fully unlock the benefits of purge separated self-limiting reactions. With the potential for direct interaction with polarizable defects and impurities and minimal substrate heating, MW-ALD is a promising new form of EE-ALD that merits further investigation.

SUPPLEMENTARY MATERIAL

Supplementary material contains a description of wafer temperature measurements made using an instrumented thermocouple

wafer and temperature stickers, before, during, and after various microwave exposure sequences.

ACKNOWLEDGMENTS

Kupp and Conley acknowledge financial support from ASMI during part of the project. This work was performed at the Materials Synthesis and Characterization (MaSC) Center, a National Science Foundation (NSF) National Nanotechnology Coordinated Infrastructure (NNCI) Northwest Nanotechnology Infrastructure (NWNI) open user facility at Oregon State University supported in part through NSF Grant No. NNCI-2025489. The authors thank Chris Tasker (MaSC) for his help with the MW system retrofit and troubleshooting.

AUTHOR DECLARATIONS

Conflict of Interest

The authors have no conflicts to disclose.

Author Contributions

Benjamin Kupp: Data curation (lead); Formal analysis (lead); Investigation (lead); Methodology (lead); Writing – original draft (lead); Writing – review & editing (supporting). **Jessica Haglund:** Data curation (supporting); Formal analysis (supporting); Investigation (equal); Writing – review & editing (supporting). **Shane Witsell:** Investigation (supporting). **Mohammad Kamarehi:** Resources (lead); Writing – review & editing (supporting). **John F. Conley Jr.:** Conceptualization (lead); Formal analysis (equal); Funding acquisition (lead); Investigation (supporting); Methodology (equal); Project administration (lead); Supervision (lead); Writing – original draft (supporting); Writing – review & editing (lead).

DATA AVAILABILITY

The data that support the findings of this study are available from the corresponding author upon reasonable request.

REFERENCES

[1]V. Vandalon and W. M. M. Kessels, Appl. Phys. Lett. **108**, 011607 (2016).
[2]M. D. Groner, F. H. Fabreguette, J. W. Elam, and S. M. George, Chem. Mater. **16**, 639 (2004).
[3]R. L. Puurunen, J. Appl. Phys. **97**, 121301 (2005).
[4]M. Hayes, M. A. Jenkins, J. Woodruff, D. F. Moser, C. L. Dezelah, and J. F. Conley, Jr., J. Vac. Sci. Technol. A **39**, 052402 (2021).
[5]J. F. Conley, Jr., Y. Ono, and D. J. Tweet, Appl. Phys. Lett. **84**, 1913 (2004).
[6]J. F. Conley, Jr., D. J. Tweet, Y. Ono, and G. Stecker, MRS Proc. **811**, 5–10 (2004).
[7]J. F. Conley, Jr., Y. Ono, D. J. Tweet, G. Stecker, R. Solanki, and W.-W. Zhuang, *Physics and Technology of High-k Gate Dielectrics II* (Electrochemical Society, Pennington, NJ, 2003), p. 11.
[8]J. F. Conley, Jr., Y. Ono, and G. Stecker, U.S. patent 7,442,415 (28 October 2008).
[9]T. Nabatame *et al.*, *2003 Symposium on VLSI Technology. Digest of Technical Papers (IEEE Cat. No. 03CH37407)*, Kyoto, Japan, June 2003 (IEEE, Piscataway, NJ, 2003), p. 25.
[10]H. Jagannathan, R. D. Clark, S. Consiglio, P. Jamison, B. Linder, M. Hopstaken, G. Leusink, V. Paruchuri, and V. Narayanan, ECS Trans. **33**, 157 (2010).
[11]R. D. Clark, S. Aoyama, S. Consiglio, G. Nakamura, and G. Leusink, ECS Trans. **35**, 815 (2011).
[12]R. D. Clark, S. Consiglio, G. Nakamura, Y. Trickett, and G. J. Leusink, ECS Trans. **41**, 79 (2011).
[13]S. Consiglio, R. D. Clark, E. Bersch, J. LaRose, I. Wells, K. Tapily, G. J. Leusink, and A. Diebold, ECS Trans. **41**, 89 (2011).
[14]K. Tapily, S. Consiglio, R. D. Clark, R. Vasić, E. Bersch, J. Jordan-Sweet, I. Wells, G. J. Leusink, and A. C. Diebold, ECS Trans. **45**, 411 (2012).
[15]T. Henke, M. Knaut, C. Hossbach, M. Geidel, L. Rebohle, M. Albert, W. Skorupa, and J. W. Bartha, ECS J. Solid State Sci. Technol. **4**, P277 (2015).
[16]M. C. Langston, N. P. Dasgupta, H. J. Jung, M. Logar, Y. Huang, R. Sinclair, and F. B. Prinz, J. Phys. Chem. C **116**, 24177 (2012).
[17]A. Delabie *et al.*, J. Electrochem. Soc. **153**, F180 (2006).
[18]H.-Y. Shih, W.-H. Lee, W.-C. Kao, Y.-C. Chuang, R.-M. Lin, H.-C. Lin, M. Shiojiri, and M.-J. Chen, Sci. Rep. **7**, 39717 (2017).
[19]M. N. Bhuyian, D. Misra, K. Tapily, R. D. Clark, S. Consiglio, C. S. Wajda, G. Nakamura, and G. J. Leusink, ECS J. Solid State Sci. Technol. **3**, N83 (2014).
[20]W.-H. Lee, Y.-T. Yin, P.-H. Cheng, J.-J. Shyue, M. Shiojiri, H.-C. Lin, and M.-J. Chen, ACS Sustain. Chem. Eng. **7**, 487 (2019).
[21]W.-C. Kao, W.-H. Lee, S.-H. Yi, T.-H. Shen, H.-C. Lin, and M.-J. Chen, RSC Adv. **9**, 12226 (2019).
[22]W.-H. Lee, W.-C. Kao, Y.-T. Yin, S.-H. Yi, K.-W. Huang, H.-C. Lin, and M.-J. Chen, Appl. Surf. Sci. **525**, 146615 (2020).
[23]S. T. Ueda *et al.*, J. Mater. Chem. C **10**, 5707 (2022).
[24]C.-Y. Wang, H.-C. Huang, C.-Y. Chou, H.-Y. Chen, C.-H. Ling, H.-C. Lin, and M.-J. Chen, ACS Appl. Electron. Mater. **5**, 2487 (2023).
[25]C.-Y. Wang, C.-Y. Chou, H.-F. Shiue, H.-Y. Chen, C.-H. Ling, J.-J. Shyue, and M.-J. Chen, Appl. Surf. Sci. **585**, 152748 (2022).
[26]T.-J. Chang, Y.-S. Jiang, S.-H. Yi, C.-Y. Chou, C.-I. Wang, H.-C. Lin, and M.-J. Chen, Appl. Surf. Sci. **591**, 153110 (2022).
[27]K. Saito, Y. Watanabe, K. Takahashi, T. Matsuzawa, B. Sang, and M. Konagai, Sol. Energy Mater. Sol. Cells **49**, 187 (1997).
[28]J.-C. Kwak, Y.-H. Lee, and B.-H. Choi, Appl. Surf. Sci. **230**, 249 (2004).
[29]S. K. Kim, S. Hoffmann-Eifert, and R. Waser, Electrochem. Solid-State Lett. **14**, H146 (2011).
[30]V. Miikkulainen, K. Väyrynen, V. Kilpi, Z. Han, M. Vehkamäki, K. Mizohata, J. Räisänen, and M. Ritala, ECS Trans. **80**, 49 (2017).
[31]K. H. Yoon, H. Kim, Y.-E. K. Lee, N. K. Shrestha, and M. M. Sung, RSC Adv. **7**, 5601 (2017).
[32]K. E. K. Holden, S. M. Witsell, P. C. Lemaire, and J. F. Conley, Jr., J. Vac. Sci. Technol. A **40**, 040401 (2022).
[33]J. Olander, L. M. Ottosson, P. Heszler, J.-O. Carlsson, and K. M. E. Larsson, Chem. Vap. Depos. **11**, 330 (2005).
[34]C. H. Liu, M. Yan, X. Liu, E. Seelig, and R. P. H. Chang, Chem. Phys. Lett. **355**, 43 (2002).
[35]J. K. Sprenger, A. S. Cavanagh, H. Sun, K. J. Wahl, A. Roshko, and S. M. George, Chem. Mater. **28**, 5282 (2016).
[36]H. B. Profijt, S. E. Potts, M. C. M. van de Sanden, and W. M. M. Kessels, J. Vac. Sci. Technol. A **29**, 050801 (2011).
[37]J. F. Conley, Jr., R. Solanki, G. Stecker, L. Charneski, W. Zhuang, D. Tweet, L. Stecker, W. Gao, and Y. Ono, "ALD of HfO_2 on a New Modulated Temperature Tool using $Hf(NO_3)_4$," paper presented at the 2002 American Vacuum Society Topical Conference on Atomic Layer Deposition (ALD 2002), Seoul, Korea, August 2002.
[38]T. Tanimura, Y. Watanabe, Y. Sato, Y. Kabe, and Y. Hirota, J. Appl. Phys. **113**, 064102 (2013).
[39]C. Fu *et al.*, AIP Adv. **7**, 035214 (2017).
[40]K. J. Rao, B. Vaidhyanathan, M. Ganguli, and P. A. Ramakrishnan, Chem. Mater. **11**, 882 (1999).
[41]K. Thompson, J. H. Booske, Y. B. Gianchandani, and R. F. Cooper, IEEE Electron Device Lett. **23**, 127 (2002).

[42]A. D. Mason, T. F. Roberts, J. F. Conley, Jr., D. T. Price, D. D. J. Allman, and M. S. McGuire, *2009 International Semiconductor Device Research Symposium*, College Park, MD, December (IEEE, Piscataway, NJ, 2009), p. 1.
[43]T. L. Alford, D. C. Thompson, J. W. Mayer, and N. D. Theodore, J. Appl. Phys. **106**, 114902 (2009).
[44]Y. Lee *et al.*, IEEE Trans. Electron Devices **61**, 651 (2014).
[45]T. Iwai, K. Eriguchi, S. Yamauchi, N. Noro, J. Kitagawa, and K. Ono, J. Vac. Sci. Technol. A **33**, 061403 (2015).
[46]T.-L. Shih, Y.-H. Su, T.-C. Kuo, W.-H. Lee, and M. I. Current, Appl. Phys. Lett. **111**, 012101 (2017).
[47]L.-F. Teng, P.-T. Liu, Y.-J. Lo, and Y.-J. Lee, Appl. Phys. Lett. **101**, 132901 (2012).
[48]C.-S. Fuh, P.-T. Liu, L.-F. Teng, S.-W. Huang, Y.-J. Lee, H.-P. D. Shieh, and S. M. Sze, IEEE Electron Device Lett. **34**, 1157 (2013).
[49]K.-W. Jo and W.-J. Cho, Appl. Phys. Lett. **105**, 213505 (2014).
[50]K.-W. Jo, S.-W. Moon, and W.-J. Cho, Appl. Phys. Lett. **106**, 043501 (2015).
[51]S. Zhao, Y. Dong, M. Yu, X. Guo, X. Xu, Y. Jing, and Y. Xia, J. Semicond. **35**, 112001 (2014).
[52]M.-S. Kang and W.-J. Cho, J. Nanosci. Nanotechnol. **19**, 6232 (2019).
[53]J. H. Bang *et al.*, Ceram. Int. **45**, 7723 (2019).
[54]R. Redko, G. Milenin, N. Safriuk-Romanenko, S. Redko, M. Semenenko, and A. Sarikov, Phys. Status Solidi A **222**, 2400863 (2025).
[55]B. Zhu, X. Wu, W.-J. Liu, S.-J. Ding, D. W. Zhang, and Z. Fan, Nanoscale Res. Lett. **14**, 53 (2019).
[56]L. Yue, C. Fu, F. Sun, Z. Qiu, S. Zhang, and D. Wu, IEEE Electron Device Lett. **38**, 1390 (2017).
[57]J. D. Kraus, Proc. IRE **36**, 1236 (1948).
[58]J. D. Kraus, Proc. IRE **37**, 263 (1949).
[59]*Antenna Engineering Handbook*, edited by R. C. Johnson and H. Jasik, 3rd ed. (McGraw-Hill, New York, 1993).
[60]O. J. Glasser and J. D. Kraus, J. Appl. Phys. **19**, 193 (1948).
[61]M. A. Lieberman and A. J. Lichtenberg, *Principles of Plasma Discharges and Materials Processing* (John Wiley & Sons, Ltd, Hoboken, 2005), p. 535.
[62]National Institute of Standards and Technology (2021).
[63]P. Xu, C. Fu, C. Hu, D. Wei Zhang, D. Wu, J. Luo, C. Zhao, Z.-B. Zhang, and S.-L. Zhang, Appl. Phys. Lett. **102**, 122114 (2013).
[64]F. Argall and A. K. Jonscher, Thin Solid Films **2**, 185 (1968).